

Comparing algorithms for diffeomorphic registration: Stationary LDDMM and Diffeomorphic Demons

Monica Hernandez¹, Salvador Olmos¹, and Xavier Pennec²

¹ Communication Technologies Group (GTC)
Aragon Institute of Engineering Research (I3A)
University of Zaragoza, Spain

² Asclepios, INRIA Sophia-Antipolis, France

Abstract. The stationary parameterization of diffeomorphisms is being increasingly used in computational anatomy. In certain applications it provides similar results to the non-stationary parameterization alleviating the computational charge. With this characterization for diffeomorphisms, two different registration algorithms have been recently proposed: stationary LDDMM and diffeomorphic Demons. To our knowledge, their theoretical and practical differences have not been analyzed yet. In this article we provide a comparison between both algorithms in a common framework. To this end, we have studied the differences in the elements of both registration scenarios. We have analyzed the sensitivity of the regularization parameters in the smoothness of the final transformations and compared the performance of the registration results. Moreover, we have studied the potential of both algorithms for the computation of essential operations for further statistical analysis. We have found that both methods have comparable performance in terms of image matching although the transformations are qualitatively different in some cases. Diffeomorphic Demons shows a slight advantage in terms of computational time. However, it does not provide as stationary LDDMM the vector field in the tangent space needed to compute statistics or exact inverse transformations.

Key words: Computational Anatomy, diffeomorphic registration, stationary parameterization, LDDMM, diffeomorphic Demons

1 Introduction

Computational Anatomy aims at the study of the statistical variability of anatomical structures [1]. Anatomical information is encoded by the spatial transformations existing between anatomical images and a template selected as reference [2]. The analysis of these transformations allows modeling the anatomical variability of a population. In particular, statistical inference can be used in order to identify anatomical differences between healthy and diseased groups or improve the diagnosis of pathologies [3–5]. In the absence of a justified physical model

for inter-subject variability, diffeomorphisms (i.e. differentiable maps with differentiable inverse) provide a convenient mathematical framework to perform this statistical analysis [6, 7].

The Large Deformation Diffeomorphic Metric Mapping (LDDMM) has been considered the reference paradigm for diffeomorphic registration in Computational Anatomy [8, 9]. Diffeomorphisms are represented as end point of paths parameterized by time-varying vector fields defined on the tangent space of a convenient Riemannian manifold. Despite the solid foundations of the mathematical framework, the high computational requirements have made this methodology not much attractive for clinical applications where more efficient registration algorithms are usually preferred.

Recently, an alternative parameterization using stationary vector fields was proposed [7]. This parameterization has been applied for diffeomorphic registration in the variational problem studied in the LDDMM framework [10, 11] and diffeomorphic Demons algorithm [12]. Stationary LDDMM is embedded into the theoretical complexity of the LDDMM framework although it has resulted into a much more efficient algorithm while providing similar registration results. Diffeomorphic Demons is intended as an extension of original Demons algorithm suitable for practical applications due to its efficiency and the quality of registration results.

Although both methods have arisen from different backgrounds, they consider non-rigid registration as a diffusion process [13]. Moreover, they fit into the same variational framework with the same image matching metric and similar characterizations for the diffeomorphic transformations. To our knowledge, the theoretical and practical differences between both methods have not been analyzed yet. In this article, we provide a comparison between both algorithms in this common framework. The elements of the registration scenario (transformation parameterization, image metric, regularization and optimization scheme) have been studied for both methods. In the experimental section we have analyzed the influence of the regularization parameters on the smoothness of the final transformations and compared the performance of the registration results. Moreover, we have studied the potential of both algorithms for the computation of the inverse transformation and the logarithm which constitute essential operations for further statistical analysis.

The rest of the article is divided as follows. In Section 2 we study the elements of stationary-LDDMM and diffeomorphic Demons. Results are presented in Section 3. Finally, Section 4 presents the main concluding remarks.

2 Stationary LDDMM and Diffeomorphic Demons

In Computational Anatomy, diffeomorphic registration is defined as a variational problem involving the characterization of diffeomorphic transformations, an image metric to measure the similarity between the images after registration, a regularization constraint to favor stable numerical solutions, and an optimization technique to search for the optimal transformation in the space of valid

diffeomorphisms. The transformation that deforms the source I_0 into the target I_1 is computed from the minimization of the energy functional

$$E(\varphi) = \frac{1}{\sigma_{\text{reg}}^2} \cdot E_{\text{reg}}(\varphi) + \frac{1}{\sigma_{\text{sim}}^2} \cdot E_{\text{sim}}(I_0, I_1, \varphi) \quad (1)$$

where the weighting factors $1/\sigma_{\text{reg}}^2$ and $1/\sigma_{\text{sim}}^2$ balance the energy contribution between regularization and matching. In this section we study the elements of this registration scenario for stationary LDDMM [10, 11] and diffeomorphic Demons [12].

2.1 Characterization of diffeomorphic transformations

In the LDDMM framework [14, 8], transformations are assumed to belong to a group of diffeomorphisms (i.e. differentiable maps $\varphi : \Omega \rightarrow \Omega$ with differentiable inverse) endowed with a Hilbert differentiable structure of Riemannian manifold, $\text{Diff}(\Omega)$. The tangent space V is a set of Sobolev class vector fields in Ω . The Riemannian metric is defined from the scalar product $\langle v, w \rangle_V = \langle \mathcal{L}v, \mathcal{L}w \rangle_{L^2}$ where \mathcal{L} is a linear invertible differentiable operator. Diffeomorphic transformations are represented by the end point $\varphi = \phi(1)$ of paths of diffeomorphisms $\phi(t)$ parameterized by time-varying flows $v(t)$ of vector fields in V from the solution of the transport equation $\dot{\phi}(t) = v(t, \phi(t))$. The Sobolev structure in V guarantees the existence of diffeomorphic solutions for these equations if $\int_0^1 \|v(t)\|_V^2 dt < \infty$.

In stationary LDDMM [10, 11], paths of diffeomorphisms are parameterized by constant-time flows of vector fields in V . This stationary parameterization is closely related to the group structure defined in $\text{Diff}(\Omega)$ as the paths starting at the identity parameterized using stationary vector fields are exactly the one-parameter subgroups. Diffeomorphisms belonging to one-parameter subgroups can be computed from the group exponential map $\text{Exp} : V \rightarrow \text{Diff}(\Omega)$

$$\varphi = \text{Exp}(w) \quad (2)$$

where w constitutes the infinitesimal generator of the subgroup [7]. Thus, stationary LDDMM restricts transformations to diffeomorphisms belonging to one-parameter subgroups. It has been shown that the set of diffeomorphisms obtained with the stationary parameterization do not comprise all diffeomorphisms in $\text{Diff}(\Omega)$ [15]. Nevertheless, the stationary parameterization has shown to provide a performance similar to the more general non-stationary parameterization on the registration of MRI brain anatomical images [11].

In diffeomorphic Demons [12], transformations are assumed to belong to a group of diffeomorphisms $\text{Diff}(\Omega)$. In contrast to the LDDMM framework, no Riemannian structure is explicitly considered in $\text{Diff}(\Omega)$. Diffeomorphic transformations are represented as the composition of

$$\varphi = \psi \circ \text{Exp}(u) \quad (3)$$

where ψ is an element in $Diff(\Omega)$ and u is a vector field in Ω belonging to a convenient space of vector fields that guarantees the existence of the exponential map and that the composition $\psi \circ \text{Exp}(u)$ remains in $Diff(\Omega)$. This characterization restricts transformations to any element in $Diff(\Omega)$ that can be obtained by finite composition of exponentials of smooth vector fields $\varphi = \text{Exp}(u_1) \circ \dots \circ \text{Exp}(u_N)$.

2.2 Image metric

In stationary LDDMM the image matching energy is defined from

$$E_{\text{sim}}(I_0, I_1, \varphi) = \|I_0 \circ \text{Exp}(w)^{-1} - I_1\|_{L^2}^2 \quad (4)$$

This term could be replaced by other energies proposed in non-stationary LDDMM (as mutual information or cross correlation, among others [16, 17]). In general, the inverse of the minimizer of $E_{\text{sim}}(I_0, I_1, \cdot)$ is not minimizing the reciprocal energy $E_{\text{sim}}(I_1, I_0, \cdot)$. Therefore, if the order of inputs is swapped the method does not provide exact inverse transformations. Introducing inverse consistency in the registration is important as the symmetry in the image matching should be guaranteed by the diffeomorphic transformations used in most of Computational Anatomy applications [17]. In stationary LDDMM, $\text{Exp}(-w)$ and $\text{Exp}(w)$ are exact inverse transformations. Therefore, the inverse consistent version of the image matching energy for stationary LDDMM simply corresponds to

$$E_{\text{sim}}(I_0, I_1, \varphi) = \|I_0 \circ \text{Exp}(w)^{-1} - I_1\|_{L^2}^2 + \|I_1 \circ \text{Exp}(w) - I_0\|_{L^2}^2 \quad (5)$$

Diffeomorphic Demons is associated to the minimization of

$$E_{\text{sim}}(I_0, I_1, \varphi) = \|I_0 \circ \psi \circ \text{Exp}(u) - I_1\|_{L^2}^2 \quad (6)$$

The inverse consistent version of the image matching energy corresponds to ³

$$E_{\text{sim}}(I_0, I_1, \varphi) = \|I_0 \circ \psi \circ \text{Exp}(u) - I_1\|_{L^2}^2 + \|I_1 \circ \zeta \circ \text{Exp}(w) - I_0\|_{L^2}^2 \quad (7)$$

subject to $(\psi \circ \text{Exp}(u))^{-1} = \zeta \circ \text{Exp}(w)$. In this case, minimization involves the solution of a constrained optimization problem leading to a more complex algorithm for general expressions of ψ and ζ .

2.3 Regularization energy

In stationary LDDMM the regularization term is defined as the norm in V of the infinitesimal generator w associated to the diffeomorphism φ , $E_{\text{reg}}(\varphi) = \|w\|_V^2 = \|\mathcal{L}w\|_{L^2}^2$. The regularization term favors solutions to belong to one-parameter subgroups with small energy preventing the transformations to be

³ The inverse $(\psi \circ \text{Exp}(u))^{-1} = \text{Exp}(-u) \circ \psi^{-1}$ is written in the form given by Eq. 3

non-diffeomorphic. The regularization term depends on the selection of the operator \mathcal{L} that is usually related to the physical deformation model imposed on Ω . However, it remains an open question how to choose the best model in non-rigid registration algorithms [13, 10]. In this work we use the diffusive model $\mathcal{L} = Id - \alpha \nabla^2$. This selection restricts w to lie on a space of Sobolev class two.

In Demons framework regularization is externally imposed using Gaussian smoothing on φ and u . This way, the physical deformation model assumed on Ω is roughly equivalent to the combination of a diffusive and a fluid model [18]. It can be shown that the effect of this Gaussian smoothing is equivalent to using the harmonic regularization $E_{\text{reg}}(\varphi) = \|D\varphi - I\|_{\text{fro}}^2$ in Eq. 1 .

2.4 Optimization scheme

In stationary LDDMM, optimization is performed on the tangent space V (optimization on Hilbert spaces). Although classical gradient descent is usually used for numerical optimization [9, 11], more efficient and robust second-order techniques have been recently proposed [10, 19]. These methods are based on Newton's iterative scheme

$$w^{k+1} = w^k - \epsilon \cdot H_w E(w^k)^{-1} \cdot \nabla_w E(w^k) \quad (8)$$

although they differ on the space where first and second order Gâteaux (i.e. directional) derivatives are computed and the simplification of the Hessian term used to overcome the numerical problems posed by Newton's method.

In [10], Gâteaux derivatives are computed on the space of square integrable functions and Levenberg - Marquardt Newton's simplification is used. Thus, the expressions for the gradient and the Hessian are given by

$$(\nabla_w E(w))_{L^2} = 2 (\mathcal{L}^\dagger \mathcal{L})w - (I_0 \circ \text{Exp}(w)^{-1} - I_1) \cdot \nabla(I_0 \circ \text{Exp}(w)^{-1}) \quad (9)$$

$$(H_w E(w))_{L^2} = 2 (\mathcal{L}^\dagger \mathcal{L}) + \nabla(I_0 \circ \text{Exp}(w)^{-1})^T \cdot \nabla(I_0 \circ \text{Exp}(w)^{-1}) \quad (10)$$

With this approach, the action of the linear operator $\mathcal{L}^\dagger \mathcal{L}$ has to be formulated using the matrix representation of the convolution. As a consequence, the algorithm results in a high dimensional matrix inversion problem with large computational requirements. Although inversion is approached by solving a sparse system of linear equations combining Gauss-Seidel with multigrid techniques [20], the memory requirements for diffeomorphic registration hinder the execution in standard machines.

As an alternative, it was proposed in [19] to compute Gâteaux derivatives in the space V using a Gauss-Newton simplification, which leads to

$$(\nabla_w E(w))_V = 2 w - (\mathcal{L}^\dagger \mathcal{L})^{-1}((I_0 \circ \text{Exp}(w)^{-1} - I_1) \cdot \nabla(I_0 \circ \text{Exp}(w)^{-1})) \quad (11)$$

$$(H_w E(w))_V = 2 I_{\mathbb{R}^3} + (\mathcal{L}^\dagger \mathcal{L})^{-2}(\nabla(I_0 \circ \text{Exp}(w)^{-1})^T \cdot \nabla(I_0 \circ \text{Exp}(w)^{-1})) \quad (12)$$

With this approach, the action of the operators $(\mathcal{L}^\dagger \mathcal{L})^{-1}$ and $(\mathcal{L}^\dagger \mathcal{L})^{-2}$ can be formulated using convolution and the update of Eq. 8 can be computed using pointwise operations with smaller memory requirements.

Apart from the computational requirements, Beg et al. provided an additional argument supporting optimization on space V rather than on L^2 [9]. The linear operator $\mathcal{K} = (\mathcal{L}^\dagger \mathcal{L})^{-1}$ is a compact operator in V . Using results from F. Riesz's spectral theory of compact operators, there exists an orthonormal basis $(\varpi_n)_{n \in \mathbb{N}}$ in L^2 with corresponding singular values $(\lambda_n)_{n \in \mathbb{N}}$ such that

$$\mathcal{K} = \sum_{n \in \mathbb{N}} (\lambda_n \langle \cdot, \varpi_n \rangle_{L^2}) \cdot \varpi_n \quad (13)$$

and $\lambda_n \rightarrow 0$ as $n \rightarrow \infty$ due to operator compactness. The expansion of the gradient expressions in this basis yields ⁴

$$(\nabla_w E(w))_{L^2} = \sum_{n \in \mathbb{N}} \left(\frac{1}{\lambda_n} \langle 2w, \varpi_n \rangle_{L^2} + \langle -b, \varpi_n \rangle_{L^2} \right) \cdot \varpi_n \quad (14)$$

$$(\nabla_w E(w))_V = \sum_{n \in \mathbb{N}} (\langle 2w, \varpi_n \rangle_{L^2} + \lambda_n \langle -b, \varpi_n \rangle_{L^2}) \cdot \varpi_n \quad (15)$$

where $b = (I_0 \circ \text{Exp}(w)^{-1} - I_1) \cdot \nabla(I_0 \circ \text{Exp}(w)^{-1})$. Therefore, whereas the action of the linear operator $(\mathcal{L}^\dagger \mathcal{L})^{-1}$ in Eq. 11 remains bounded, the action of $(\mathcal{L}^\dagger \mathcal{L})$ Eq. 9 results into a high frequency components amplification leading to numerical instabilities in the computations.

In diffeomorphic Demons optimization is performed on the group of diffeomorphisms $\text{Diff}(\Omega)$ (optimization on Lie groups) using the iterative scheme

$$u^{k+1} = \frac{I_0 \circ \varphi^k - I_1}{\|\nabla(I_0 \circ \varphi^k) \cdot D\varphi^k\|_{L^2}^2 + (I_0 \circ \varphi^k - I_1)^2 / \tau^2} \cdot (\nabla(I_0 \circ \varphi^k) \cdot (D\varphi^k)) \quad (16)$$

$$\varphi^{k+1} = \varphi^k \circ \text{Exp}(\epsilon \cdot u^{k+1}) \quad (17)$$

where second order techniques are used for the computation of u^k [12].

Regularization is performed at the end of each iteration by smoothing the updated u^k and φ^k using Gaussian filters of standard deviation σ_u and σ_φ , respectively. Moreover, the term $(I_0 \circ \varphi^k - I_1)^2 / \tau^2$ also contributes to the regularization by enforcing the numerical stability of the optimization scheme and controlling the maximum update step length. This term can be seen as a Levenberg - Marquardt approximation of Gauss-Newton's method. Leaving aside the common variational formulation provided in this work, an identical optimization scheme can be obtained from a variational formulation resulting from the introduction of a hidden variable that controls the correspondences between φ and the true transformation [21].

Alternative to this usual Gauss-Newton optimization, the efficient second order scheme introduced in [22] was used in [12]. This led to replacing the term $\nabla(I_0 \circ \varphi)$ in Eq. 16 by its symmetric version $\nabla(I_0 \circ \varphi) + \nabla I_1$. This was shown to improve the rate of convergence with respect to the original Gauss-Newton

⁴ Analogous conclusions can be inferred from expanding the bilinear form associated to Hessian expressions in this basis.

Table 1. Stationary LDDMM registration. Average and standard deviation of the RSSD (%) (upper row) and J_{\min} (lower row) for different values of the regularization parameters α and $1/\sigma_{\text{sim}}^2$. The optimal result for each algorithm is outlined in bold-face. Non-diffeomorphic results are outlined in italics. Note that the algorithms do not converge for values α of order 0.0001.

		Inverse consistent LDDMM. $RSSD = \frac{1}{2} \frac{\ I_0 \circ \varphi - I_1\ _2^2 + \ I_1 \circ \varphi^{-1} - I_0\ _2^2}{\ I_0 - I_1\ _2^2}$.						
$1/\sigma_{\text{sim}}^2 \backslash \alpha$		1.0	0.01	0.0050	0.0025	0.0010	0.0001	
1.0e3		91.56 ± 3.04	30.53 ± 3.76	21.51 ± 2.37	17.42 ± 4.16	<i>12.18 ± 3.17</i>	100.00 ± 0.00	
		0.60 ± 0.24	0.44 ± 0.11	0.27 ± 0.07	0.17 ± 0.06	<i>-0.17 ± 0.64</i>	1.00 ± 0.00	
1.0e4		90.97 ± 3.11	24.70 ± 3.10	17.55 ± 2.10	13.88 ± 4.13	<i>9.72 ± 3.72</i>	100.00 ± 0.00	
		0.59 ± 0.24	0.31 ± 0.15	0.19 ± 0.08	0.10 ± 0.05	<i>-3.97 ± 12.28</i>	1.00 ± 0.00	
1.0e5		90.97 ± 3.11	24.70 ± 3.10	17.55 ± 2.10	13.82 ± 4.00	<i>9.61 ± 3.57</i>	100.00 ± 0.00	
		0.59 ± 0.24	0.31 ± 0.15	0.19 ± 0.08	0.10 ± 0.05	<i>-3.99 ± 12.28</i>	1.00 ± 0.00	

		Symmetric gradient LDDMM. $RSSD = \frac{\ I_0 \circ \varphi - I_1\ _2^2}{\ I_0 - I_1\ _2^2}$.						
$1/\sigma_{\text{sim}}^2 \backslash \alpha$		1.0	0.01	0.0050	0.0025	0.0010	0.0001	
1.0e3		91.66 ± 2.88	30.44 ± 3.44	22.02 ± 2.33	15.79 ± 1.68	<i>10.88 ± 1.21</i>	100.00 ± 0.00	
		0.65 ± 0.22	0.44 ± 0.09	0.26 ± 0.08	0.11 ± 0.07	<i>0.02 ± 0.02</i>	1.00 ± 0.00	
1.0e4		91.11 ± 2.73	28.61 ± 3.44	20.99 ± 2.38	14.81 ± 1.59	<i>10.09 ± 1.35</i>	100.00 ± 0.00	
		0.63 ± 0.23	0.39 ± 0.12	0.23 ± 0.10	0.10 ± 0.07	<i>0.01 ± 0.01</i>	1.00 ± 0.00	
1.0e5		91.11 ± 2.73	28.83 ± 3.62	21.49 ± 2.46	15.38 ± 2.74	<i>10.09 ± 1.34</i>	100.00 ± 0.00	
		0.63 ± 0.23	0.39 ± 0.12	0.25 ± 0.10	0.11 ± 0.07	<i>0.01 ± 0.01</i>	1.00 ± 0.00	

scheme. It should be noted that the efficient second order scheme can be also introduced in Gauss-Newton LDDMM optimization by modifying Eqs. 9 to 12. In the experimental section, we will explore its influence in registration results.

3 Results

3.1 Datasets and experimental setting

A set of 18 T1-MRI images from the Internet Brain Segmentation Repository (IBSR) were used for comparing the performance of the registration algorithms. The images size was $256 \times 256 \times 128$ with a voxel size of $0.94 \times 0.94 \times 1.5$. The images were acquired at the Massachusetts General Hospital and are freely available at <http://www.cma.mgh.harvard.edu/ibsr/data.html>.

In our experiments, one of the images was randomly selected as a template and the remaining of the datasets were registered to this template using stationary LDDMM and diffeomorphic Demons algorithms. Both algorithms were stopped when the magnitude of the update was negligible or after a maximum of 100 iterations. The selection of the optimal regularization parameters is presented below. Other parameters were fixed to typical values used in previous works [10–12]. The parameter ϵ controls the step size made along the search direction in both methods. It was estimated using a backtracking inexact line-search strategy starting from $\epsilon = 1$ for each iteration (see [19] for more details).

Stationary LDDMM was implemented with the scheme given in Eq. 11 and 12. Both the inverse consistent version of the algorithm IC-LDDMM (Eq. 5), and the symmetric gradient optimization scheme SG-LDDMM (use of $\nabla I_0 \circ \text{Exp}(w)^{-1} + \nabla I_1$ instead of $\nabla I_0 \circ \text{Exp}(w)^{-1}$ in the optimization scheme) have been considered in the study. Diffeomorphic Demons was run with the symmetric gradient as proposed in [12].

3.2 Regularization parameters selection

The selection of the regularization parameters is crucial in deformable registration. Strong regularization constraints hinder large deformations and provide a poor intensity match. In contrast, parameters leading to a weak regularization do not constrain the deformation enough and often lead to non diffeomorphic results. The criteria for parameter selection depends on the application. In this work, we wanted to find a tradeoff that provided the best intensity match with minimum deformation. The Relative Sum of Squared Differences (RSSD) between the images before and after registration was used to quantify the image match while Deformation was measured using the Jacobian minimum.

In LDDMM regularization parameter α determine the shape of the kernels associated to the linear operators $(\mathcal{L}^\dagger \mathcal{L})^{-1}$ and $(\mathcal{L}^\dagger \mathcal{L})^{-2}$ in the Fourier domain. Therefore, the selection of α is crucial on the smoothness of the velocity field w . The lower values of α the higher frequency components are conserved on w thus allowing larger deformations. As α goes to 0, the linear operators become close to the identity leading to negligible regularization and non-diffeomorphic solutions. In this work we fixed the parameter $1/\sigma_{\text{reg}}^2$ to 1.0 in order to handle the parameters selection more easily and studied the influence of α and $1/\sigma_{\text{sim}}^2$ on registration results. Table 1 shows the metrics for parameter selection for different values of these parameters. This led us to select $\alpha = 0.0025$ and $1/\sigma_{\text{sim}}^2 = 1.0e4$.

In diffeomorphic Demons, parameters σ_φ and σ_u control the smoothness of the diffeomorphism φ and the velocity field u , respectively. Therefore, the lower values of σ the higher frequency components are conserved on φ and u allowing larger deformations. In addition, the maximum step length is bounded by $\|u\| \leq 0.5 \cdot \tau$. As τ increases, the maximum magnitude of the velocity field u remains unbounded which can lead to non-diffeomorphic solutions. In this work we fixed the parameters $1/\sigma_{\text{reg}}^2$ and σ_φ to 1.0 mm. Table 2 shows the metrics for parameter selection for different values of σ_u and τ . Optimal values are obtained for $\sigma_u = 1.0$ mm. (close to voxel size) and $\tau = 0.5$ mm.

3.3 Registration results

We have measured the quality of the image matching and the transformations after registration for stationary LDDMM and diffeomorphic Demons. The image matching has been assessed from the RSSD associated to φ and φ^{-1} . For the quantification of the transformations quality we have considered the regularization energies associated to both variational problems, $\|\cdot\|_V^2$ and $\|\cdot\|_{\text{fro}}^2$. In

Table 2. Diffeomorphic Demons registration. Average and standard deviation of the RSSD (%) (upper row) and J_{\min} (lower row) for different values of the regularization parameters σ_{sim} and τ . The optimal result is outlined in boldface. Non-diffeomorphic results are outlined in italics.

		Diffeomorphic Demons. $RSSD = \frac{\ I_0 \circ \varphi - I_1\ _2^2}{\ I_0 - I_1\ _2^2}$.				
$\tau \backslash \sigma_u$		1.0	1.5	2.0	2.5	3.0
0.5	RSSD	14.88 ± 1.74	20.91 ± 2.50	31.58 ± 3.67	40.71 ± 4.34	48.15 ± 4.61
	J_{\min}	0.07 ± 0.03	0.15 ± 0.04	0.31 ± 0.05	0.47 ± 0.06	0.59 ± 0.06
1.0	RSSD	<i>9.95 ± 1.18</i>	<i>13.99 ± 1.69</i>	<i>21.73 ± 2.73</i>	<i>29.37 ± 3.72</i>	<i>36.19 ± 4.47</i>
	J_{\min}	<i>0.00 ± 0.00</i>	<i>0.02 ± 0.02</i>	0.11 ± 0.05	0.23 ± 0.07	0.35 ± 0.09
2.0	RSSD	<i>10.91 ± 1.79</i>	<i>12.60 ± 1.26</i>	<i>18.06 ± 2.15</i>	24.51 ± 3.01	30.59 ± 3.75
	J_{\min}	<i>-0.01 ± 0.02</i>	<i>-0.00 ± 0.01</i>	0.02 ± 0.02	0.10 ± 0.04	0.19 ± 0.07

stationary LDDMM φ and φ^{-1} have been computed from the exponential map of w [7]. In diffeomorphic Demons the inverse diffeomorphism and the vectors in the tangent space have been computed as proposed in [7]. Table 3 presents the results of these metrics. In addition, Figure 1 shows the registration results for the experiment with the largest ventricle deformation. Figure 2 shows some representative examples of the image-based energy curves during optimization.

3.4 Efficiency

Our experiments were performed on a 2.33 GHZ machine with a C++ implementation based on the ITK library. We found that the computation time per iteration was approximately 41.54 seconds for diffeomorphic Demons, 53.23 seconds for SG-LDDMM and 90.64 seconds for IC-LDDMM. However, it should be noted that if we were also interested in computing the inverse diffeomorphism or the logarithm from the output of diffeomorphic Demons, the computation time of the inverse diffeomorphism would take in average 5706 ± 34 seconds whereas the computation time for the logarithm would take 17463 ± 10681 seconds.

Table 3. Average and standard deviation of the metrics associated to the registration results. With IC-LDDMM and SG-LDDMM we indicate the inverse consistent and the symmetric gradient version of LDDMM, respectively.

	$RSSD_{(I_0 \circ \varphi, I_1)}$ (%)	$RSSD_{(I_1 \circ \varphi^{-1}, I_0)}$ (%)	$\ \cdot\ _V^2$	$\ \cdot\ _{\text{fro}}^2$
IC-LDDMM	13.42 ± 4.23	14.43 ± 4.24	140.52 ± 28.84	0.17 ± 0.05
SG-LDDMM	14.81 ± 1.59	15.47 ± 2.50	166.62 ± 12.05	0.20 ± 0.03
Demons	14.88 ± 1.74	19.00 ± 4.72	2626.70 ± 6069.90	0.13 ± 0.01

4 Discussion and conclusions

In this article we presented a theoretical and experimental comparison of two diffeomorphic registration techniques that use stationary vector fields to compute diffeomorphisms. We analyzed the differences in the elements of both registration scenarios, studied the influence of the regularization parameters on the quality of the final transformations and compared the performance of the registration results. For stationary LDDMM, we considered both the inverse consistent version of the algorithm and the symmetric gradient optimization scheme.

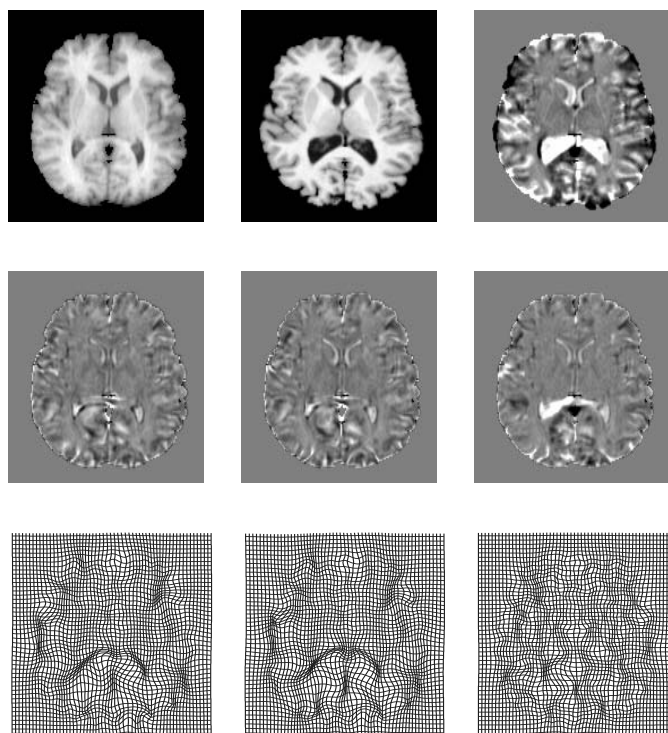


Fig. 1. Visual assessment of diffeomorphic registration algorithms. First row shows axial slices of the reference (left) and the deforming image (middle) together with the differences before registration (right). Second row shows the differences after registration with IC-LDDMM (left), SG-LDDMM (middle) and Demons (right). Third row shows the corresponding diffeomorphisms.

For diffeomorphic Demons we just considered the symmetric gradient optimization scheme. We found that parameters α in LDDMM and τ in diffeomorphic Demons were strongly influencing the smoothness of the final transformation. There even exist combinations of such parameters that provide non diffeomorphic transformations. It seems that non diffeomorphic transformations at RSSD approximately below 13% can be achieved in our datasets. This should be taken into account in parameter selection for specific applications.

We found that both algorithms provided a similar intensity matching (average RSSD ranging from 13.42 to 14.88 %). However, in some cases, both algorithms locally showed different performance. As can be appreciated in Figure 1, larger deformations in stationary LDDMM yielded a higher image matching in locations such as, for example, ventricles tails. SG-LDDMM provided a slightly better consistent inverse image matching than diffeomorphic Demons (average RSSD of 15.5 for stationary LDDMM vs RSSD of 19.0 for Demons). In this case, average RSSD differences between methods were statistically different for diffeomorphic Demons. The regularization energy in V showed to be much higher in the case of diffeomorphic Demons. This may be due to the bad numerical con-

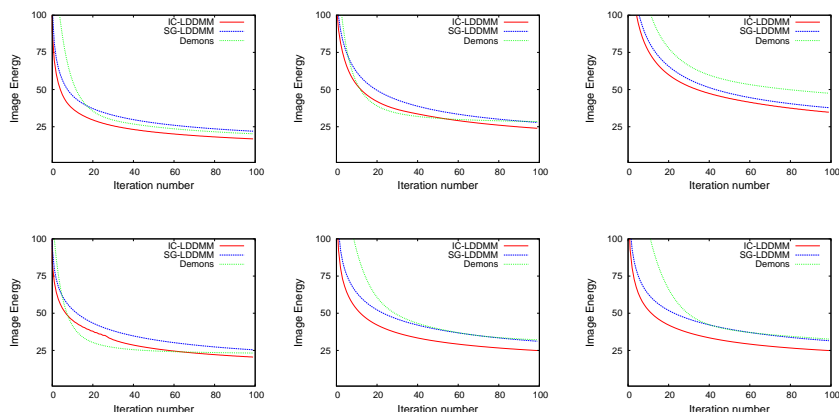


Fig. 2. Representative examples of the image matching curves during optimization.

ditioning of the logarithm map computation or to the absence of smoothness constraints on the second order derivatives of the transformations. As shown in Figure 2, IC-LDDMM provided the highest rate of convergence in all cases. At the initial stages of optimization, diffeomorphic demons showed the worst performance in the great majority of cases although it usually reached SG-LDDMM performance at convergence.

Diffeomorphic Demons was 1.28 times faster than SG-LDDMM and 2.18 times faster than IC-LDDMM. However, it should be noted that stationary LDDMM provides elements on the tangent space instead of transformations as output. This allows to compute exponentials and inverses with a low computational cost. On the contrary, diffeomorphic Demons only provides transformations as output. Therefore, logarithms and inverses have to be estimated using quite computationally expensive iterative algorithms.

In conclusion, both methods may be considered close from a theoretical point of view and equivalent from a practical point of view for registration purposes. Diffeomorphic Demons demonstrated similar intensity matching performances to stationary LDDMM at a slightly lower computational cost. It should be advisable to select this algorithm for registration applications where the efficiency of the algorithm is crucial, while stationary LDDMM should be selected for applications where either the transformation smoothness or the inverse consistency is important, or if the inverse transformations or logarithm maps need to be computed. The selection between SG-LDDMM or IC-LDDMM would again depend on the trade-off between computation time and accuracy for the specific application.

References

1. Grenander, U., Miller, M.: Computational Anatomy: an emerging discipline. *Quart. Appl. Math.* **56** (1998) 617 – 694

2. Grenander, U.: General pattern theory. Oxford University Press (1994)
3. Thompson, P.M., et al.: Detection and mapping of abnormal brain structure with a probabilistic atlas of cortical surfaces. *J. Comp. Ass. Tomography* **21**(4) (1997) 567 – 581
4. Thompson, P.M., et al.: Cortical change in Alzheimer’s disease detected with a disease-specific population-based brain atlas. *Cerebral Cortex* **11**(1) (2001) 1 – 16
5. Miller, M.I.: Computational anatomy: shape, growth, and atrophy comparison via diffeomorphisms. *Neuroimage* **23** (2004) 19–33
6. Miller, M.I., Troune, A., Younes, L.: Geodesic shooting for computational anatomy. *J. Math. Imaging Vis.* **24** (2006) 209–228
7. Arsigny, V., Commonwicz, O., Pennec, X., Ayache, N.: Statistics on diffeomorphisms in a Log-Euclidean framework. *MICCAI’06, LNCS* **4190** (2006) 924 – 931
8. Dupuis, P., Grenander, U., Miller, M.: Variational problems on flows of diffeomorphisms for image matching. *Quart. Appl. Math.* (1998) 587 – 600
9. Beg, M., Miller, M., Troune, A., Younes, L.: Computing large deformation metric mappings via geodesic flows of diffeomorphisms. *Int. J. Comput. Vis.* **61** (2) (2005) 139–157
10. Ashburner, J.: A fast diffeomorphic image registration algorithm. *Neuroimage* **38**(1) (2007) 95 – 113
11. Hernandez, M., Bossa, M.N., Olmos, S.: Registration of anatomical images using geodesic paths of diffeomorphisms parameterized with stationary vector fields. *MMBIA’07* (2007)
12. Vercauteren, T., Pennec, X., Perchant, A., Ayache, N.: Diffeomorphic image registration with the demons algorithm. *MICCAI’07, LNCS* **4792** (2007) 319 – 326
13. Modersitzki, J.: Numerical methods for image registration. Oxford University Press (2004)
14. Troune, A.: Diffeomorphism groups and pattern matching in image analysis. *Int. J. Comput. Vis.* **28** (1998) 213 – 221
15. Grabowski, J.: Free subgroups of diffeomorphism groups. *Fundam. Math.* **131** (1988) 103 – 121
16. Lorenzen, P., Prastawa, M., Davis, B., Gerig, G., Bullitt, E., Joshi, S.: Multi-modal image set registration and atlas formation. *Med. Image. Anal.* **10** (2006) 440 – 451
17. Avants, B.B., Epstein, C.L., Grossman, M., Gee, J.C.: Symmetric dieomorphic image registration with cross-correlation: Evaluating automated labeling of elderly and neurodegenerative brain. *Med. Image. Anal.* **12** (1998) 26 – 41
18. Pennec, X., Cachier, P., Ayache, N.: Understanding the Demons algorithm: non-rigid registration by gradient descent. *MICCAI’99, LNCS* **1679** (1999) 597 – 605
19. Hernandez, M., Olmos, S.: Gauss-Newton optimization in diffeomorphic registration. *ISBI’08* (2008)
20. Press, W.H., Teukolsky, S.A., Vetterling, W.T., Flannery, B.P.: Numerical recipes in C: the art of scientific computing. Cambridge University Press, Cambridge (1992)
21. Cachier, P., Bardinnet, E., Dormont, D., Pennec, X., Ayache, N.: Iconic feature based nonrigid registration: the PASHA algorithm. *Comput. Vis. Image Underst.* **89** (2003) 272 – 298
22. Malis, E.: Improving vision-based control using efficient second-order minimization techniques. *IEEE Int. Conf. Robot. Aut.* **2** (2004) 1843 – 1848